PAN ARCHIVES OF ACOUSTICS
Vol. 41, No. 1, pp. 27–41 (2016)

DOI: 10.1515/aoa-2016-0003

Research Papers

Prediction of Reverberant Properties of Enclosures via a Method Employing a Modal Representation of the Room Impulse Response

Mirosław MEISSNER

Institute of Fundamental Technological Research, Polish Academy of Sciences
Pawińskiego 5B, 02-106 Warszawa, Poland; e-mail: mmeissn@ippt.pan.pl

(*received May 11, 2015; accepted July 23, 2015*)

A theoretical method has been presented to describe sound decay in enclosures and simulate the room impulse response (RIR) employed for prediction of the indoor reverberation characteristics. The method was based on a solution of wave equation with the form of a series whose time-decaying components represent responses of acoustic modes to an impulse sound source. For small sound absorption on room walls this solution was found by means of the method of variation of parameters. A decay function was computed via the time-reverse integration of the squared RIR. Computer simulations carried out for a rectangular enclosure have proved that the RIR function reproduces the structure of a sound field in the initial stage of sound decay sufficiently well. They have also shown that band-limitedness of the RIR has evident influence on the shape of the decay function and predicted decay times.

Keywords: room acoustics, indoor reverberation, room impulse response, modal expansion method, decay times.

1. Introduction

One of the most primary aims of room acoustics is prediction of reverberant properties of enclosures from measured or numerically simulated room responses because reverberation is the most basic and easily perceived acoustical feature of rooms. Description of a sound field in enclosures and evaluation of their reverberant characteristics are not simple, and several theoretical methods of different complexity have been developed for this. They utilize statistical-acoustic methods, diffusion-equation model, geometric acoustics methods, wave-based methods, and modal expansion methods. Statistical-acoustic methods (Summers *et al.*, 2004; Summers, 2012) are based on the diffuse sound field hypothesis that the acoustic energy is uniform in the field and travels in all directions with the same probability. The diffusion-equation model (Xiang *et al.*, 2009; Luizard *et al.*, 2014) is an extension of the statistical theory to spatially varying reverberant sound fields and is based on the analogy of the sound energy density with a density of "sound particles" travelling along straight lines. The geometric acoustics methods are adequate for high sound frequencies and most systems for geometric modelling are based on the ray tracing method (Summers *et al.*, 2005), the beam tracing algorithm (Funkhouser *et al.*, 2004; Laine *et al.*, 2009), the image source method (Dance *et al.*, 1995; Lehmann, Johansson, 2009), or the mirror source method (Mechel, 2002; Aretz *et al.*, 2014). The fact that geometric methods do not include directly wave phenomena such as interferences or diffraction is a considerable disadvantage. Therefore, the results obtained with such methods are inaccurate for enclosures with complex shapes, such as L- and U-shaped rooms, and for enclosures consisting of coupled rooms.

Wave-based methods, in contrast to geometric approaches, solve the wave equation after suitable discretization to describe a complete sound field in enclosed spaces. The most common among these numerical techniques are the finite element method (FEM) (Easwaran, Craggs, 1996a; Okuzono *et al.*, 2014), the boundary element method (BEM) (Franzoni *et al.*, 2001; Sakuma, Yasuda, 2002), and the finite-difference time-domain (FDTD) method (López *et al.*, 2013; Murphy *et al.*, 2014). Alternatives to the FDTD technique are the pseudospectral time-domain (PSTD)

method (Spa *et al.*, 2010) and adaptive rectangular decomposition (ARD) (Raghuvanshi *et al.*, 2009), which achieve a good accuracy with a much coarser spatial discretization. All these wave-based methods provide different advantages and disadvantages depending on their complexity and computational load. However, the most important difference lies in their applicability: the frequency domain methods, such as FEM and BEM, typically provide results for steady-state situations, whereas the time domain models, such as FDTD, make it possible to predict impulse responses of enclosures (Sakamoto *et al.*, 2008). Wave-based methods can also be successfully applied to partially bounded spaces (Szemela, 2015).

Modal expansion methods are techniques used for vibration analysis of mechanical objects and structures, thus, they have been applied in several branches of technical sciences. In room acoustics, these methods yield the resonant modes of pressure vibrations in a room, and the pressure field in the room is expressed as a linear combination of the resonant modes (Meissner, 2010; Dance, Van Buuren, 2013). The most common among these methods are the normal mode analysis (Morse, Bolt, 1944), which is the oldest and simplest type of modal analysis, the classical modal analysis (Dowell, 1978) developed by using the Green's theorem, the asymptotic modal analysis (Kubota, Dowell, 1992), and the hybrid modal analysis (Xu, Sommerfeldt, 2010) that combines the free field Green's function and a modal expansion. Methods employing the modal expansion approach are more difficult to apply for rooms with complex shapes (Li, Cheng, 2004; Sum, Pan, 2006) but it fully describes the wave nature of a sound field such as degeneration of modes (Meissner, 2009a) and modal localization (Félix *et al.*, 2007; Meissner, 2009b), as well as creation of energy vortices in the sound intensity field (Meissner, 2012; 2015a). Their disadvantages are a significant increase in computation times at higher frequencies, usually slow convergence speed, and occurrence of modal coupling in the case of the classical modal analysis.

Reverberation time is the main parameter determining the indoor reverberation characteristics, thus, it is primarily used to assess the acoustic quality of enclosures. However, in many practical cases determination of several different decay times is necessary because in the low-frequency range the sound decay behavior is usually non-exponential. In theoretical models the decay times are evaluated from a decay curve defined as the graphical representation of the decay of the sound pressure level in a room as a function of time after the cut-off of a continuous sound source (ISO 3382, 2012). The estimation of decay times is achieved by approximation of appropriate parts of the decay curve by fitting lines obtained by a least-squares regression and then calculation of decay times from the slope of these lines (Meissner, 2013a; 2015b). Another method of determining the decay curve consists in the reverse-time integration of the squared room impulse response (RIR). This technique results in a statistically stable estimate of the sound decay because the obtained decay plot corresponds to the average over infinitely many decay curves that would be obtained with bandpass-filtered noise as an excitation signal (Schroeder, 1965). The great advantage of this method is that it produces smooth monotonic decay curves, making determination of the decay times simple and accurate.

The paper presents a novel technique for a numerical prediction of reverberant properties of enclosures. The method is suitable for buildings' rooms of an arbitrary shape and is alternative to the time-domain models, such as FDTD, which are able to predict transient responses of rooms. The method exploits a modal representation of the RIR obtained by solving the wave equation for an enclosure subjected to a time impulse. The sound absorption on the room walls was assumed to be small because the proposed method is designed for lightly damped room systems. A decay function employed for evaluating the decay times was found via a backward integration of the squared RIR. A numerical analysis of the sound decay inside a rectangular enclosure was executed to examine the impact of modal damping on the decay times and to test the presented method with respect to the computational load. The simulation results proved that the RIR function is able to reconstruct the impulse source and early reflections of the sound waves from the room walls, and the visualization of a sound field is more faithful when band-limitedness of the RIR becomes smaller. To properly characterize reverberant properties of the room, four decay times were calculated based on changes in the decay function. The obtained results discovered a substantial impact of band-limitedness of the RIR on the shape of the decay function and values of the decay times.

2. Theoretical modelling of the indoor reverberation

2.1. Modal representation of the room impulse response

For an arbitrarily shaped enclosure a theoretical description of the room response to a point source generating a time impulse at t_0 is based on a solution of the wave equation

$$\nabla^2 p - \frac{1}{c^2}\frac{\partial^2 p}{\partial t^2} = -\delta(t-t_0)\delta(\mathbf{r}-\mathbf{r}_0), \tag{1}$$

where $\nabla^2 = \boldsymbol{\nabla}\cdot\boldsymbol{\nabla}$ is the Laplacian ($\boldsymbol{\nabla}$ is the nabla vector operator, the dot is a scalar product), $p(\mathbf{r},t)$ is the sound pressure, c is the sound speed, δ is the

Dirac delta function, $\mathbf{r} = (x, y, z)$ is the receiving point, and the source point $\mathbf{r}_0 = (x_0, y_0, z_0)$ is located inside the room volume V. The pressure p must satisfy the causality condition. The initial conditions are defined for the time t_0 which means that $p(\mathbf{r}, t_0)$ and $p'(\mathbf{r}, t_0) = \partial p(\mathbf{r}, t)/\partial t|_{t=t_0}$ are given. According to the modal approach, the solution of Eq. (1) can be expressed as a linear combination of the mode shape functions Φ_m

$$p(\mathbf{r}, t) = \sum_{m=1}^{M} P_m(t)\Phi_m(\mathbf{r}), \tag{2}$$

where P_m are time-dependent modal amplitudes and M is the number of modes included in the series expansion (theoretically, M approaches infinity). The functions $\Phi_m(\mathbf{r})$ fulfill the orthonormal property in the room volume V

$$\int_V \Phi_m \Phi_n \,\mathrm{d}v = \delta_{mn}, \tag{3}$$

where δ_{mn} is the Kronecker delta function, and they satisfy the eigenvalue equations

$$\nabla^2 \Phi_m + \left(\frac{\omega_m}{c}\right)^2 \Phi_m = 0, \tag{4}$$

where ω_m is the m-th natural eigenfrequency. If it is assumed that the room walls are locally reacting to the pressure, then the boundary condition that must be satisfied on the surface S of room walls is as follows

$$\boldsymbol{\nabla} p \cdot \mathbf{n} = -\frac{\beta}{c}\frac{\partial p}{\partial t}, \tag{5}$$

where $\mathbf{n}$ is the unit vector normal to the walls which is directed away from the room volume and β is the specific wall admittance. In the following it will be assumed that a sound damping inside a room is small. In this case the room walls are characterized by a low absorption: $\mathrm{Re}(\beta) \ll 1$, thus, it is possible to assume that space distributions of modes are well approximated by uncoupled mode shape functions computed for hard room walls (Dowell *et al.*, 1977). Enclosures with such absorption properties are known in the literature as lightly damped rooms (Easwaran, Craggs, 1996b; Dance, Van Buuren, 2013).

A method for finding an equation for the modal amplitude P_m relies on suitable transformation of the wave equation (1). Firstly, multiply both sides of Eq. (1) by $\Phi_m(\mathbf{r})$ and integrate over the room volume V, and use the formula: $\iiint_V \Phi_m(\mathbf{r})\delta(\mathbf{r} - \mathbf{r}_0)\,\mathrm{d}v = \Phi_m(\mathbf{r}_0)$ to evaluate the delta function integral. This gives

$$\iiint_V \Phi_m \frac{\partial^2 p}{\partial t^2}\,\mathrm{d}v - c^2 \iiint_V \Phi_m \nabla^2 p \,\mathrm{d}v = c^2 \delta(t - t_0)\Phi_m(\mathbf{r}_0). \tag{6}$$

The application of Eqs. (2) and (3) in the first volume integral in Eq. (6), and the utilization of Eqs. (2)–(5) and the Green's theorem (Morse, Feshbach, 1953)

$$\iiint_V \left(p\nabla^2\Phi_m - \Phi_m \nabla^2 p\right)\,\mathrm{d}v = \iint_S \left(p\boldsymbol{\nabla}\Phi_m - \Phi_m \boldsymbol{\nabla} p\right)\cdot \mathbf{n}\,\mathrm{d}s \tag{7}$$

in the second volume integral leads to the following equation for the modal amplitude P_m

$$\frac{\partial^2 P_m}{\partial t^2} + 2r_m \frac{\partial P_m}{\partial t} + \omega_m^2 P_m = c^2 \delta(t - t_0)\Phi_m(\mathbf{r}_0), \tag{8}$$

where r_m represents the modal damping coefficient for the m-th mode

$$r_m = \frac{c}{2}\iint_S \beta \Phi_m^2 \,\mathrm{d}s. \tag{9}$$

By using the method of variation of parameters (Collins, 2006), the general solution of Eq. (8) was found as (Meissner, 2013b)

$$\begin{aligned} P_m(t) = {} & \frac{\left[x_m(t)y_m'(t_0) - y_m(t)x_m'(t_0)\right] P_m(t_0)}{W_m(t_0)} \\ & - \frac{\left[x_m(t)y_m(t_0) - y_m(t)x_m(t_0)\right] P_m'(t_0)}{W_m(t_0)} \\ & - c^2\Phi_m(\mathbf{r}_0)\left[x_m(t)\int_{t_0}^{t} \frac{\delta(\tau - t_0)y_m(\tau)}{W_m(\tau)}\,\mathrm{d}\tau \right. \\ & \left. - y_m(t)\int_{t_0}^{t} \frac{\delta(\tau - t_0)x_m(\tau)}{W_m(\tau)}\,\mathrm{d}\tau\right], \end{aligned} \tag{10}$$

where the functions $x_m(t) = e^{(-r_m - \mathrm{j}\Omega_m)t}$ and $y_m(t) = e^{(-r_m + \mathrm{j}\Omega_m)t}$ constitute a fundamental set of solutions of the homogeneous differential equation

$$\frac{\partial^2 P_m}{\partial t^2} + 2r_m \frac{\partial P_m}{\partial t} + \omega_m^2 P_m = 0, \tag{11}$$

the function $W_m(t) = x_m y_m' - x_m' y_m$ is the Wronskian of $x_m(t)$ and $y_m(t)$, $P_m(t_0)$ and $P_m'(t_0)$ are the initial conditions for the m-th mode and the quantity

$$\Omega_m = \sqrt{\omega_m^2 - r_m^2} \tag{12}$$

is the eigenfrequency for oscillations with damping, also called the damped natural eigenfrequency. After using the functions $x_m(t)$ and $y_m(t)$ in Eq. (10) one can obtain

$$P_m(t) = e^{-r_m(t-t_0)}\Bigg\{P_m(t_0)\cos[\Omega_m(t-t_0)] + \frac{r_m P_m(t_0) + P'_m(t_0)}{\Omega_m}\sin[\Omega_m(t-t_0)]\Bigg\} - \frac{\mathrm{j}c^2\Phi_m(\mathbf{r}_0)}{2\Omega_m}\Bigg[e^{\mathrm{j}\Omega_m t}\int_{t_0}^{t}\delta(\tau-t_0)e^{(r_m-\mathrm{j}\Omega_m)\tau}\,\mathrm{d}\tau - e^{-\mathrm{j}\Omega_m t}\int_{t_0}^{t}\delta(\tau-t_0)e^{(r_m+\mathrm{j}\Omega_m)\tau}\,\mathrm{d}\tau\Bigg]. \quad (13)$$

Since the integrals in Eq. (13) have the lower limit corresponding exactly to the peak of the source function, the integration should be carried out from $t_0^- = t_0 - \epsilon$, where ϵ is positive and goes to zero. In this case the integration interval includes the time at which the Dirac delta function peaks and $P_m(t_0^-)$ and $P'_m(t_0^-)$ are equal to zero, due to the causality condition. Thus, the modal amplitude for an ideal time impulse is the following:

$$P_m(t) = \frac{c^2 e^{-r_m(t-t_0)}\sin[\Omega_m(t-t_0)]\Phi_m(\mathbf{r}_0)}{\Omega_m}. \quad (14)$$

Additionally, the modal amplitude must fulfill the condition that P_m and $\partial P_m/\partial t$ are zero for $t < t_0$ because, if the impulse occurs at t_0, no effects of the impulse should be present at the earlier time. Finally, it should be proved that the modal amplitude from Eq. (14) satisfies the continuity condition at t_0. To do this, it must be assumed that in Eq. (13) the time t_0 is replaced by $t_0^+ = t_0 + \epsilon$. In this case the integrals in Eq. (13) are zero because the time t_0 is outside the integration interval, thus, the modal amplitude is determined by the initial conditions only. Using Eq. (14) it is easy to find that $\lim_{\epsilon\to 0} P_m(t_0^+) = 0$ and $\lim_{\epsilon\to 0} P'_m(t_0^+) = c^2\Phi_m(\mathbf{r}_0)$, therefore the function $P_m(t)$ obtained from Eq. (13) is the same as in Eq. (14).

An insertion of Eq. (14) into Eq. (2) enables determining the Green's function G depending on the space coordinates $\mathbf{r}$ and $\mathbf{r}_0$ and the time variables t and t_0. When it is assumed that the spatial and temporal properties of a sound source are characterized by the function $q(\mathbf{r}, t)$, then, according to the Green's function theory (Morse, Feshbach, 1953), the pressure room response to this excitation is described by the equation

$$p(\mathbf{r}, t) = \iiint_V \int_{-\infty}^{t} q(\mathbf{r}_0, t_0) G(\mathbf{r}, t|\mathbf{r}_0, t_0)\,\mathrm{d}t_0\,\mathrm{d}v_0. \quad (15)$$

An equivalent expression for the pressure $p(\mathbf{r}, t)$ can be also determined by using the convolution integral in the time domain (Kuttruff, 2009)

$$p(\mathbf{r}, t) = \iiint_V q(\mathbf{r}_0, t) * h(\mathbf{r}_0, \mathbf{r}, t)\,\mathrm{d}v_0 = \iiint_V \int_{-\infty}^{t} q(\mathbf{r}_0, t_0) h(\mathbf{r}_0, \mathbf{r}, t - t_0)\,\mathrm{d}t_0\,\mathrm{d}v_0, \quad (16)$$

where the symbol $*$ denotes the convolution operation and the function h describes the room impulse response (RIR) between the sound source at the position $\mathbf{r}_0$ and the receiver located at the point $\mathbf{r}$. From Eqs. (2), (14)–(16) it is easy to deduce that the RIR has the form

$$h(\mathbf{r}_0, \mathbf{r}, t) = c^2 \sum_{m=1}^{M} \frac{e^{-r_m t}\sin(\Omega_m t)\Phi_m(\mathbf{r}_0)\Phi_m(\mathbf{r})}{\Omega_m}. \quad (17)$$

The right-hand side of Eq. (17) is a symmetric function of the source and receiver points coordinates, thus, the RIR satisfies the reciprocity principle.

2.2. Determination of the decay function

When the room is excited by the time impulse, the procedure for describing the process of the sound decay bases on the reverse-time integration of the squared RIR (Schroeder, 1965). This method is commonly known as the Schroeder integration and it results in a smoothed decay plot from which the decay times can be directly estimated. Usually, the normalized version of the Schroeder integration method is used to determine the decay function L_d describing the sound energy decrease in a logarithmic scale

$$L_d(t) = 10\log\left[\frac{w(t)}{w(0)}\right], \quad (18)$$

where the function $w(t)$ is expressed by

$$w(t) = \int_t^{\infty} h^2(\mathbf{r}_0, \mathbf{r}, \tau)\,\mathrm{d}\tau. \quad (19)$$

After inserting Eq. (17) into Eq. (19) and calculating the integral, one can obtain

$$w(t) = \frac{c^2}{2}\sum_{i=1}^{M}\sum_{j=1}^{M}\frac{e^{-(r_i+r_j)t}}{\Omega_i\Omega_j}\Phi_i(\mathbf{r}_0)\Phi_j(\mathbf{r}_0)\Phi_i(\mathbf{r})\Phi_j(\mathbf{r}) \times \big\{A_{ij}\cos[(\Omega_i-\Omega_j)t] - B_{ij}\sin[(\Omega_i-\Omega_j)t] - C_{ij}\cos[(\Omega_i+\Omega_j)t] + D_{ij}\sin[(\Omega_i+\Omega_j)t]\big\}, \quad (20)$$

where the coefficients A_{ij}, B_{ij}, C_{ij}, and D_{ij} are given by

$$A_{ij} = \frac{r_i + r_j}{(r_i+r_j)^2 + (\Omega_i-\Omega_j)^2}, \qquad B_{ij} = \frac{\Omega_i - \Omega_j}{(r_i+r_j)^2 + (\Omega_i-\Omega_j)^2}, \quad (21)$$

$$C_{ij} = \frac{r_i + r_j}{(r_i + r_j)^2 + (\Omega_i + \Omega_j)^2}, \qquad D_{ij} = \frac{\Omega_i + \Omega_j}{(r_i + r_j)^2 + (\Omega_i + \Omega_j)^2}. \tag{22}$$

A procedure for predicting the decay times is based on finding fit lines to appropriate parts of the decay function L_d and it is realized by the linear regression.

3. Numerical simulation

The aim of the computer simulation was to predict the reverberant properties of an exemplary enclosure and test the numerical algorithm with respect to the computational load. In general, the proposed method is valid for rooms of an arbitrary shape. However, to perform numerical tests for a wide range of modal frequencies, a simple rectangular enclosure was considered because resonant vibrations in such a room are well understood and described. The room space was assumed to have the dimensions: $l_x = 8$ m, $l_y = 5$ m, $l_z = 3$ m. The room was excited by the sound source located at the point: $x_0 = 2$ m, $y_0 = 3$ m, $z_0 = 1$ m. A computer program was developed to calculate the RIR from Eq. (19) and then to evaluate the decay times from changes in the decay function L_d. Since a lightly damped room is considered, the eigenfunctions Φ_m are approximated by the mode shape functions determined for hard room walls

$$\Phi_{n_x n_y n_z}(x,y,z) = \sqrt{\frac{\epsilon_{n_x}\epsilon_{n_y}\epsilon_{n_z}}{V}} \cos\left(\frac{n_x \pi x}{l_x}\right) \cos\left(\frac{n_y \pi y}{l_y}\right) \cos\left(\frac{n_z \pi z}{l_z}\right), \tag{23}$$

where the modal indices n_x, n_y, n_z are non-negative integers and they are not simultaneously equal to zero (the trivial solution of the wave equation was excluded), $\epsilon_{n_s} = 1$ if $n_s = 0$, and $\epsilon_{n_s} = 2$ if $n_s > 0$. Inserting Eq. (21) into Eq. (4) yields the following formula for natural frequencies of acoustic modes:

$$f_{n_x n_y n_z} = \frac{c}{2}\sqrt{(n_x/l_x)^2 + (n_y/l_y)^2 + (n_z/l_z)^2}. \tag{24}$$

In the numerical study, a uniform distribution of the sound absorption on the room walls was considered. The specific wall admittance β was assumed to satisfy the condition $\mathrm{Re}(\beta) \ll 1$ because a lightly damped room was considered. Furthermore, it was postulated that $\mathrm{Re}(\beta) \gg \mathrm{Im}(\beta)$, which means that β can be represented by the specific wall conductance γ only. In this case a relationship between the random-incident absorption coefficient α_r and γ is expressed by (Kinsler *et al.*, 2000)

$$\alpha_r = 8\gamma\,[1 + \gamma/(1+\gamma) - 2\gamma \ln(1 + 1/\gamma)]. \tag{25}$$

It was also assumed that absorption properties of the room walls are slightly frequency-dependent because such a behavior is typical for well-reflecting surfaces. By inserting Eq. (23) into Eq. (9) it is easy to find that the modal damping coefficient is given by

$$r_{n_x n_y n_z} = 2\gamma c\,[H(n_x)/l_x + H(n_y)/l_y + H(n_z)/l_z], \tag{26}$$

where H is the unit step function determined by $H(x) = \frac{1}{2}[1 + \mathrm{sgn}(x)]$. Thus, for rooms of the rectangular shape the damping coefficient has seven different values for modes with nonzero natural eigenfrequency. In computer simulations, the specific wall conductance γ was set to 0.01, which is a value sufficiently small to consider the analyzed enclosure as a lightly damped room system. By virtue of Eq. (25), this value of γ corresponds to the random-incident absorption coefficient α_r of 0.073.

The number M of modes in the series on the right-side of Eq. (17) is an important parameter in the numerical study because it strongly influences the calculation time and determines the frequency band in which prediction of the decay times is possible. Now, if the frequency $f_{n_x n_y n_z}$ is smaller than the cutoff frequency f_c, then, according to Kuttruff (2009), the number M of modes within the frequency band $(0, f_c)$ is given by

$$M = \frac{4\pi V}{3}\left(\frac{f_c}{c}\right)^3 + \frac{\pi S}{4}\left(\frac{f_c}{c}\right)^2 + \frac{L}{8}\left(\frac{f_c}{c}\right), \tag{27}$$

where $V = l_x l_y l_z$ and $S = 2(l_x l_y + l_x l_z + l_y l_z)$ are the room volume and surface of the room walls, respectively, and $L = 4(l_x + l_y + l_z)$ is the sum of the lengths of the room edges. As it results from Eq. (27), the number M of modes with natural frequencies within a fixed frequency bandwidth increases with the third power of the frequency when the natural frequency is sufficiently large. This means that at higher natural frequencies the room modes significantly overlap with each other. It is commonly assumed that the frequency

$$f_{\mathrm{s}} = \frac{\sqrt{6}c}{\sqrt{\iint\limits_S \alpha_r \,\mathrm{d}s}}, \tag{28}$$

determined by Schroeder (1996), represents the transition boundary between the modal region where the room modes are well separated and the region of diffuse behavior of a sound field, known also as the Schroeder region (Skålevik, 2011), where there is a high overlap of the room modes. When the sound decay begins after turning off the low-frequency pure-tone source, it is appropriate to assume that the number M corresponds to the last mode whose frequency is smaller than the Schroeder frequency f_{s} (Meissner, 2013b), since the room modes from the Schroeder region have a negligible effect on the sound decay. It results from the fact that the reverberation process is

dominated by the modes with the natural frequencies close to the source frequency. However, when the sound decay is initiated by the time impulse, many modes contribute to the room response according to Eq. (17). Therefore, in the numerical study it was assumed that the cutoff frequency f_c can exceed the Schroeder frequency.

3.1. Visualization of the sound source and early reflections

The RIR function $h(\mathbf{r}_0, \mathbf{r}, t)$ is a solution of the wave equation in the time interval starting from $t = 0$. Therefore, it must be able to reconstruct the impulse source as well as early reflections of sound waves from the room walls. Note that Eq. (17) enables one to calculate the RIR within a fixed frequency bandwidth and this fact is of great importance in a reconstruction of the sound source in time and space. This is confirmed by the calculation results in Fig. 1 showing changes in $h/h_{\max}$ at the source position, i.e., for $\mathbf{r} = \mathbf{r}_0$, in the time interval from 0 to 30 ms for the frequency f_c of 750 Hz, 1500 Hz, and 3000 Hz. These values of f_c correspond to the number M of modes of 5864, 44440, and 345825. For larger values of f_c the numerical algorithm becomes much less effective because of a fast decrease of the computational speed.

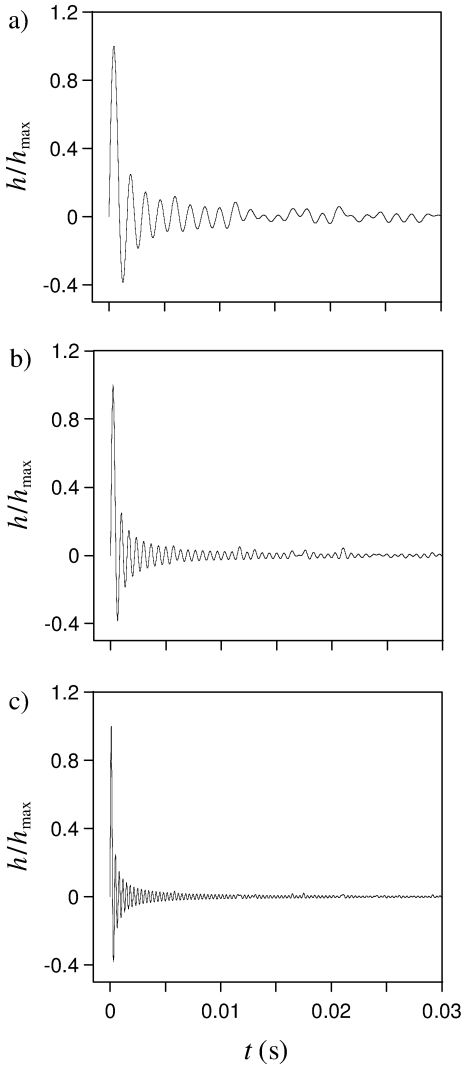

Fig. 1. Temporal changes in $h/h_{\max}$ at the source point: $x_0 = 2$ m, $y_0 = 3$ m, $z_0 = 1$ m, for the cutoff frequency f_c: a) 750 Hz, b) 1500 Hz, c) 3000 Hz.

The simulation results in Fig. 1 demonstrate that an increase in the frequency f_c moves the graphs of the RIR function towards smaller values of t and this change proceeds in such a way that a peak of the RIR occurs for a constant value of the product $f_c t$ (about 0.33). Thus, from a theoretical view point, a reconstruction of the source emitting an ideal time impulse is possible if the RIR is band-unlimited, meaning that the number M of the modes tends to infinity. The band-limitedness of the RIR also influences the spatial reconstruction of the source. This is clearly shown in Fig. 2 depicting the spatial distribution of $h/h_{\max}$ on the horizontal plane including the source point ($z = 1$ m). The values of the frequency f_c are the same as before and for each of f_c the time t satisfies the condition $f_c t = 0.33$. The simulation data in Fig. 2 demonstrate that a two-fold increase in the cutoff frequency f_c results in an approximately two-fold increase in the impulse narrowness.

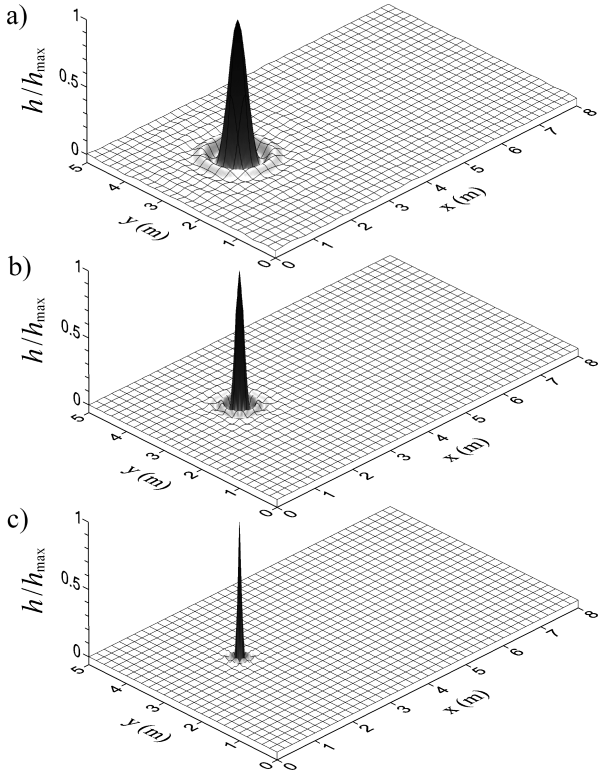

Fig. 2. Spatial distribution of $h/h_{\max}$ on the observation plane $z = 1$ m for the cutoff frequency f_c: a) 750 Hz, b) 1500 Hz, c) 3000 Hz, and the time t satisfying the condition $f_c t = 0.33$.

A sound transmission inside the room was examined in the horizontal plane 0.5 m above the source plane ($z = 1.5$ m). In this case, a square of $h/h_{\max}$ equivalent to the sound energy was calculated in order to better reconstruct the wave fronts. The calculations were performed for the cutoff frequency f_c of 3000 Hz. Figure 3 shows the wave fronts in the observation plane at very short times after the emission of the impulse source. Figure 3a depicts the wave front just after the signal emitted by the source reaches the observation plane, Fig. 3b illustrates a growth of the wave front with the progress of the time, and Fig. 3c shows the wave front just before a reflection of the direct sound from the lateral walls. For larger times the arrangement of the wave fronts is much more complex due to sound reflections. Therefore, it is more convenient to use a two-dimensional visualization of the simulation data in the form of a "snapshot" of the wave fronts in the time lapse after the first sound reflection. The calculation results presented in this way are shown in Fig. 4. They were obtained for the time t from the time interval 7–10 ms and illustrate the reflections of the direct sound from the lateral walls (Figs. 4a and 4f), a reflection of the direct sound from the floor (Fig. 4b), and a reflection of the sound, which was reflected from the floor, from two lateral walls (Fig. 4f).

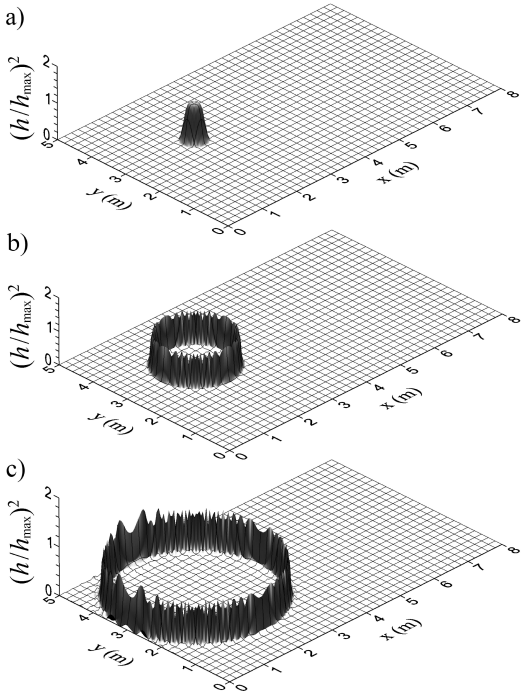

Fig. 3. Spatial distribution of $(h/h_{\max})^2$ on the observation plane $z = 1.5$ m for the time t: a) 1.5 ms, b) 3 ms, c) 5.8 ms. The cutoff frequency f_c of 3000 Hz.

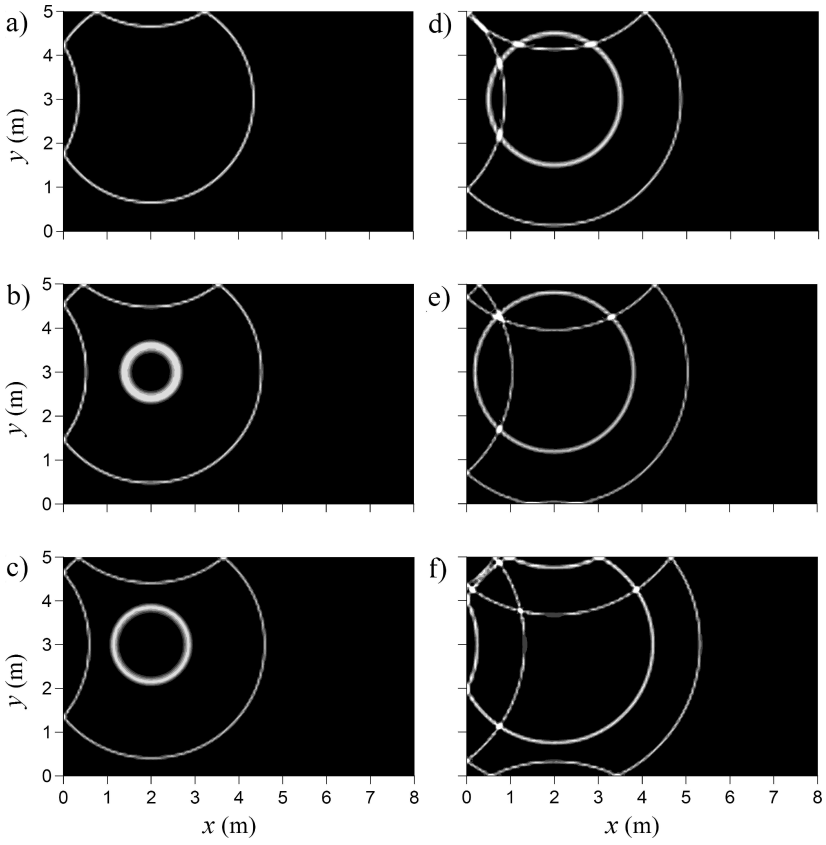

Fig. 4. Mapped distribution of $(h/h_{\max})^2$ on the observation plane $z = 1.5$ m for the time t: a) 7 ms, b) 7.5 ms, c) 7.7 ms, d) 8.5 ms, e) 9 ms, f) 10 ms. The cutoff frequency f_c of 3000 Hz.

3.2. Prediction of the decay times

Equation (17) determines the decay function L_d obtained via the backward integration of the squared RIR. Based on changes in this function, the decay times EDT, T_{10}, T_{30}, and LDT were evaluated on the observation plane $z = 1.5$ m lying 0.5 m above the source plane. The early decay time (EDT) is defined as the decay time predicted from a decrease in L_d from 0 to -10 dB, multiplied by the factor of 6. T_{10} is defined as the decay time estimated from a drop of L_d from -5 to -15 dB, multiplied by the factor of 6. Further, T_{30} is the decay time estimated from a decrease in L_d from -5 to -35, multiplied by the factor of 2. Finally, the late decay time (LDT) is defined as the decay time with the limits of -25 and -35 dB in the decay function L_d, multiplied by the factor of 6. In order to determine the decay times, the linear regression was used for finding fit lines to appropriate parts of the decay function L_d. It is important to note that both decay times EDT and T_{10} characterize a decrease in the sound energy level during the initial decay of sound. However, EDT is much more influenced by early reflections than T_{10} because, as found by Bradley and Wang (2010), the ratio LDT/T_{10} should be equal to one when the sound decay is exponential, but this may not necessarily occur with the ratio LDT/EDT.

The calculation results showing distributions of the decay times on the observation plane $z = 1.5$ m for three different values of the cutoff frequency f_c are depicted in Figs. 5–7. The plots in these figures have a form of filled contour maps which are a two-dimensional representation of three-dimensional data. As it may be seen, the distributions of the decay times are highly irregular despite the fact that a uniform distribution of the sound absorption by the room walls was assumed. They are also influenced by the number M of modes in a series expansion of the RIR because they change significantly as the frequency f_c increases. Another interesting property is a decrease in the decay times with an increase of the value of f_c. This regularity can be noted by comparing Figs. 5–7 and it is evidently seen in Table 1 depicting the ranges of the decay times for the considered values of f_c.

Equations (18)–(20) indicate that the observed variations in the decay times result from a dependence of the RIR function on the receiver position. In addition, these changes follow from the fact that the RIR is bandpass filtered because it is determined for modes with the natural frequencies $f_{n_x n_y n_z}$ smaller than the cutoff frequency f_c. Another problem, which is worth to consider, is the character of the sound decay at the receiver location because differences between decay times during the early and late stages of the decay may affect the assessment of the acoustic quality of a room (Bradley, Wang, 2005, 2010; Ermann, 2007). This issue has been analyzed for two receiving positions: $x = 4$ m, $y = 2$ m, $z = 1.5$ m and $x = 7$ m, $y = 4$ m, $z = 1.5$ m, where the minimal and maximal values of the decay times were noted. The simulation

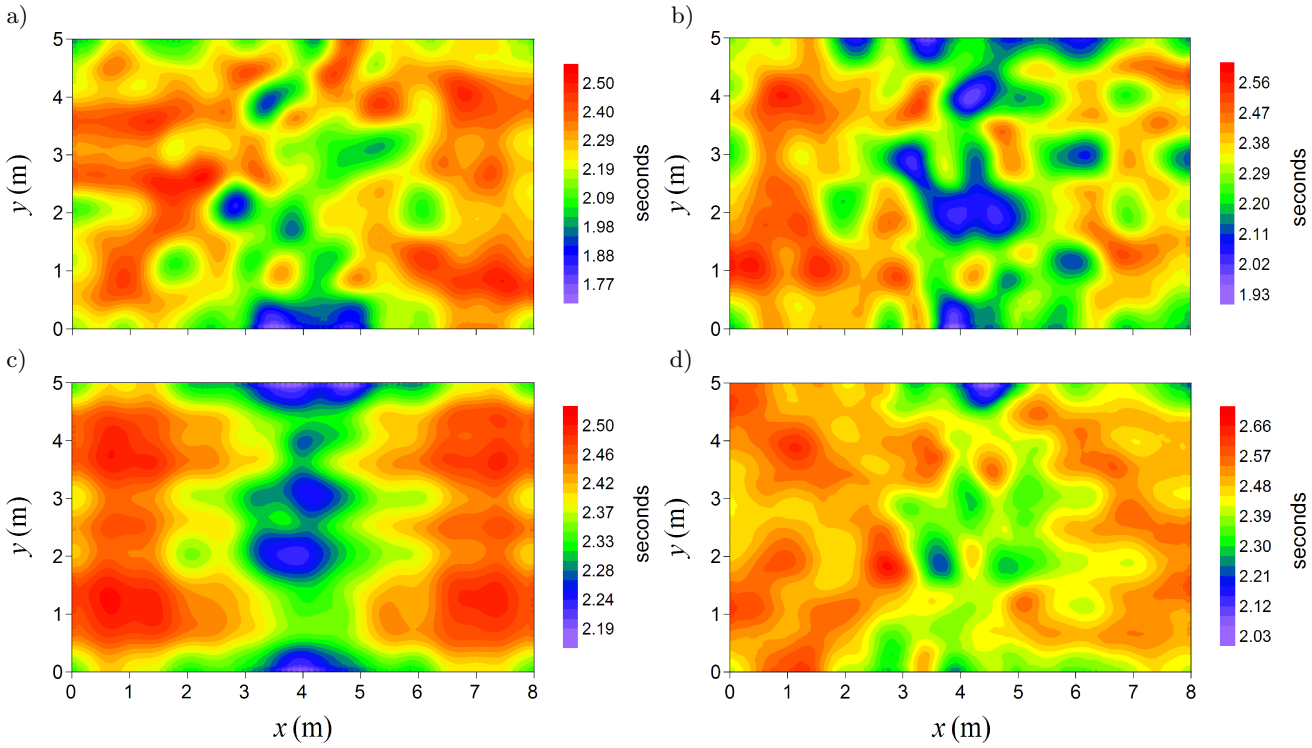

Fig. 5. Mapped distribution of decay times: a) EDT, b) T_{10}, c) T_{30}, d) LDT, on the observation plane $z = 1.5$ m for the cutoff frequency f_c of 250 Hz.

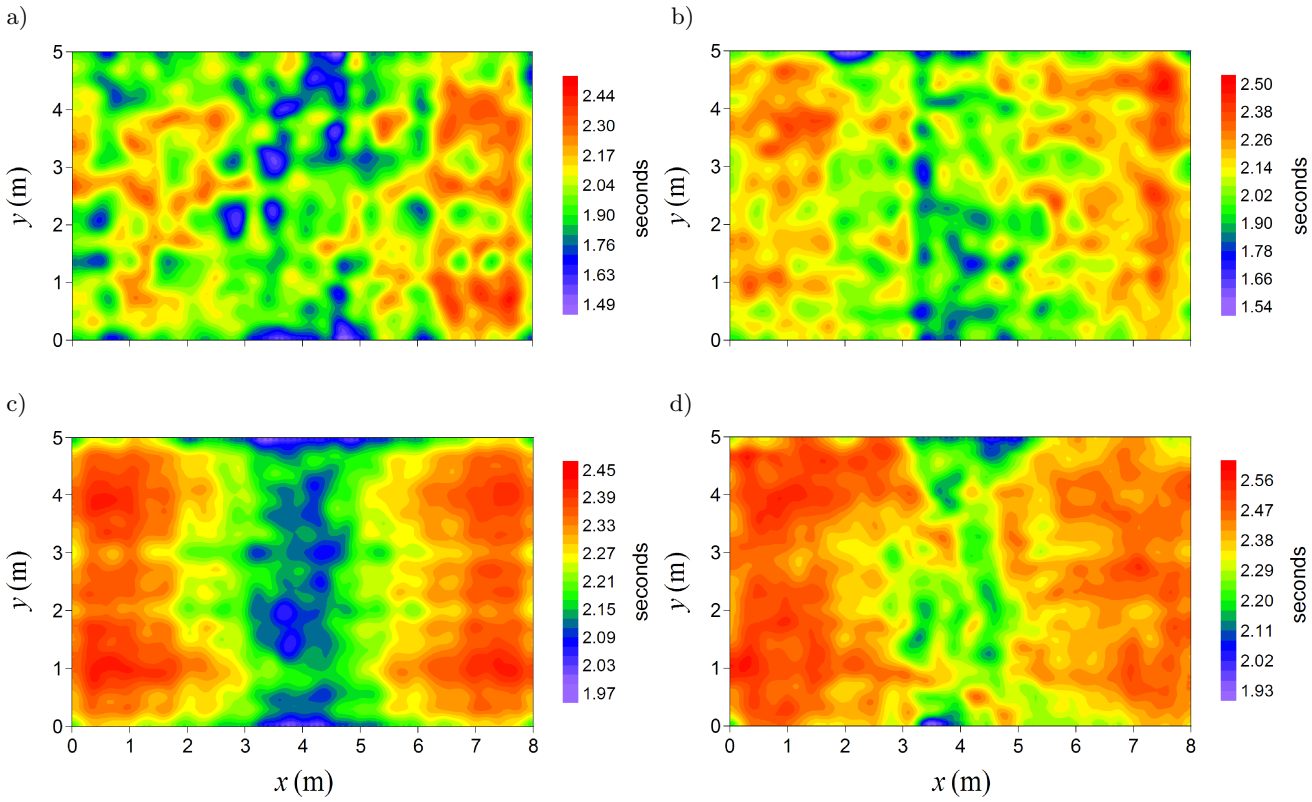

Fig. 6. Mapped distribution of decay times: a) EDT, b) T_{10}, c) T_{30}, d) LDT, on the observation plane $z = 1.5$ m for the cutoff frequency f_c of 500 Hz.

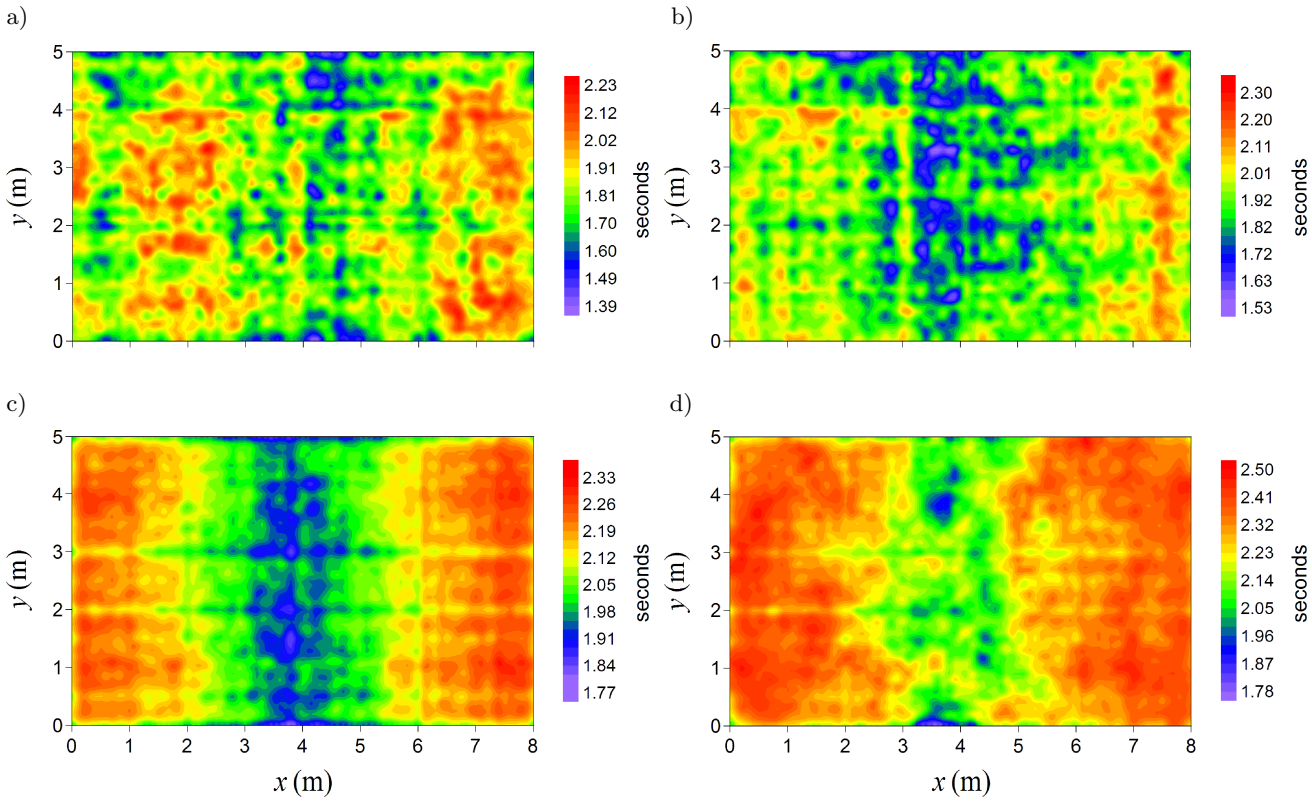

Fig. 7. Mapped distribution of decay times: a) EDT, b) T_{10}, c) T_{30}, d) LDT, on the observation plane $z = 1.5$ m for the cutoff frequency f_c of 1000 Hz.

Table 1. Ranges of the decay times EDT, T_{10}, T_{30}, and LDT on the observation plane $z = 1.5$ m for different values of the cutoff frequency f_c.

f_c [Hz]	Decay times in seconds			
	EDT	T_{10}	T_{30}	LDT
250	1.77–2.52	1.94–2.58	2.18–2.51	2.05–2.67
500	1.48–2.46	1.56–2.48	1.98–2.43	1.91–2.58
1000	1.36–2.20	1.54–2.30	1.80–2.31	1.75–2.49

results obtained at these points are shown in Figs. 8 and 9. They illustrate the changes in $h/h_{\max}$ and the decay function L_d over time for the values of f_c previously considered and provide information about the predicted decay times. The simulation data give an insight into the nature of sound decay, in particular, they indicate that, regardless of the character of temporal changes in the RIR, the Schroeder integration method creates a monotonic and smooth decay function which allows an easy estimation of the decay times. The calculation results also demonstrate the regularity that the estimated decay times decrease with increasing of the cutoff frequency f_c. Moreover, in all cases the observed changes in the decay function F_d are almost linearly dependent on the time, suggesting a nearly exponential nature of the sound decay.

The regularity that the decay times depend on the cutoff frequency f_c is connected with the structure of the room impulse response because the RIR is, in fact, a superposition of the reverberant responses of the individual modes. In a rectangular room there are three fundamental groups of modes: the axial modes (two modal indices are zero), the tangential modes (one modal index is zero), and the oblique modes (all modal indices are nonzero). A reverberant behavior of the modes is characterized by the modal decay time given by (KUTTRUFF, 2009)

$$T_{\mathrm{mod}} = \frac{3\ln(10)}{r_{n_x n_y n_z}}, \tag{29}$$

where the modal damping coefficient $r_{n_x n_y n_z}$ is determined by Eq. (24). Thus, for the analyzed rectangular room there are only seven different values of the modal decay time. These values are collected in Fig. 10a

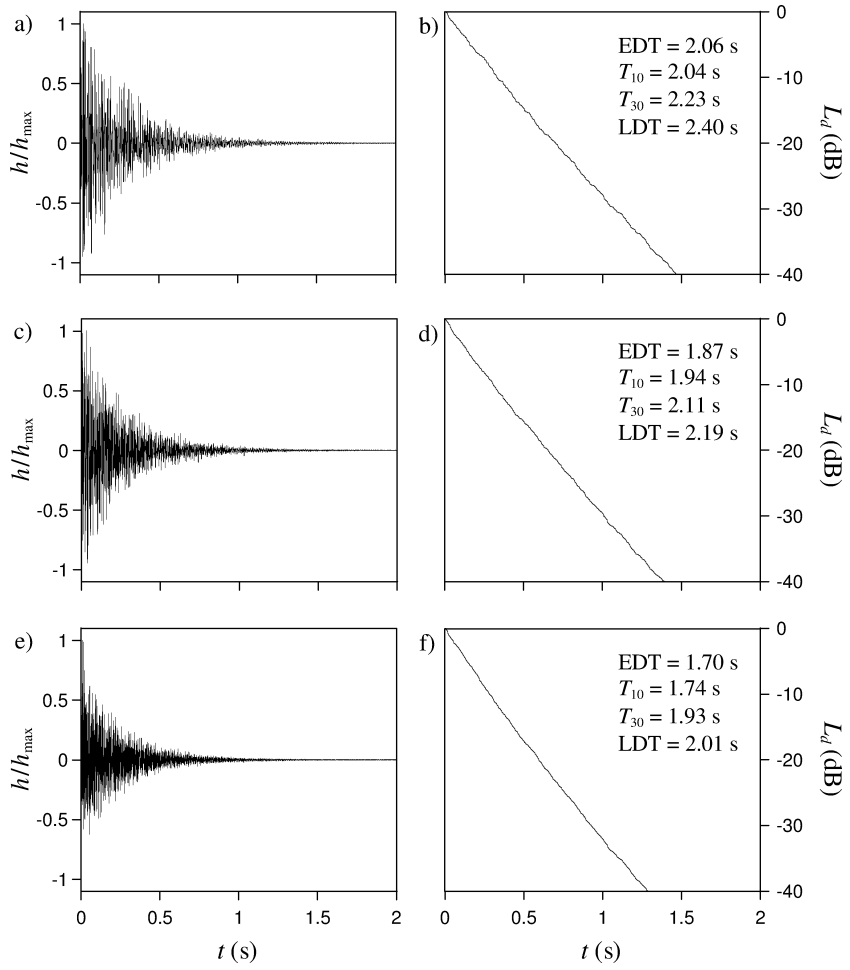

Fig. 8. Changes in $h/h_{\max}$ and the decay function L_d over time at the receiving point: $x = 4$ m, $y = 2$ m, $z = 1.5$ m, for the cutoff frequency f_c: a), b) 250 Hz, c), d) 500 Hz, e), f) 1000 Hz.

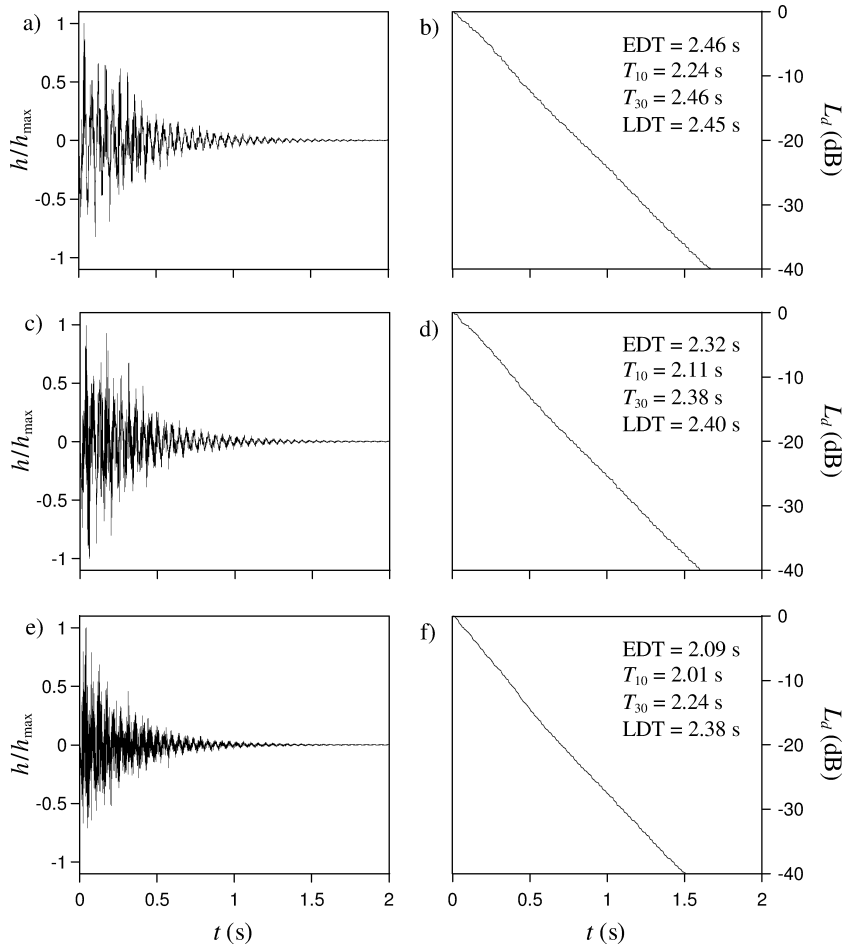

Fig. 9. Changes in $h/h_{\max}$ and the decay function L_d over time at the receiving point: $x = 7$ m, $y = 4$ m, $z = 1.5$ m, for the cutoff frequency f_c: a), b) 250 Hz, c), d) 500 Hz, e), f) 1000 Hz.

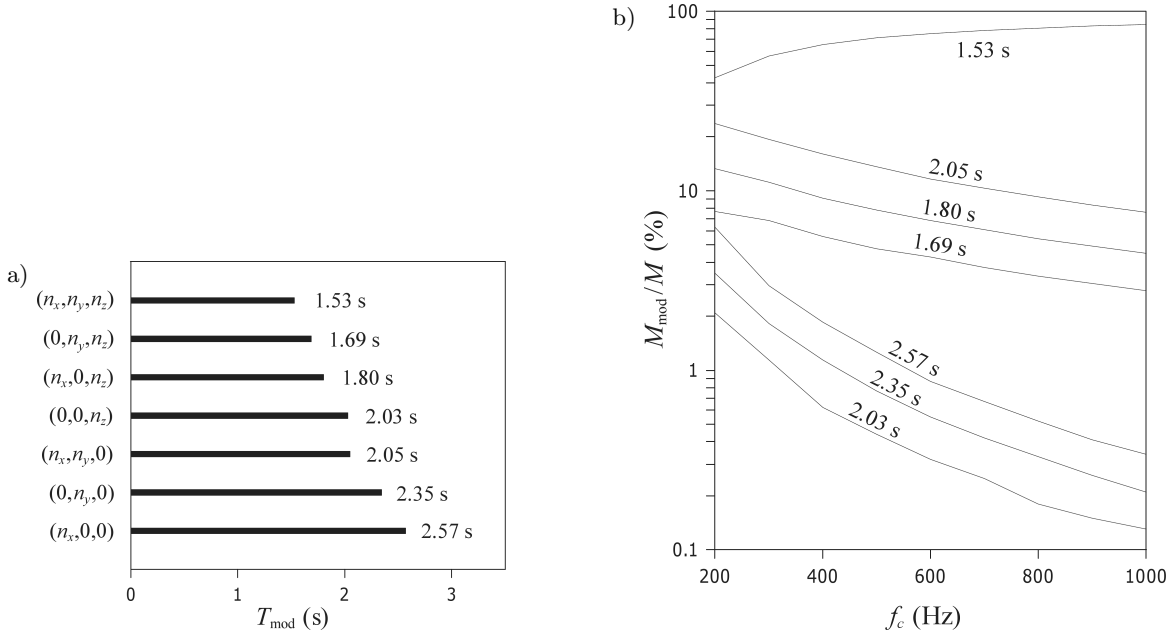

Fig. 10. a) Modal decay time T_{mod} for different types of modes, b) changes in the ratio M_{mod}/M with increasing the cutoff frequency f_c.

together with the corresponding modal indices defining the type of modes. These data show that T_{mod} is the biggest for the axial modes and the smallest for the oblique modes. The time behavior of the RIR depends on the fact of which types of modes are dominant during a sound decay. Since the RIR is determined by a series then it is reasonable to assume that the ratio between the number M_{mod} of modes of a given type and the number M of all modes in the series is an indicator of a modal influence on the RIR. The number M is related to the cutoff frequency f_c via Eq. (27), then, knowing M_{mod}, it is easy to find the dependence of the ratio M_{mod}/M on the frequency f_c for each type of modes. The calculation results presented in Fig. 10b prove that a contribution of axial and tangential modes in the RIR is relatively small and the ratio M_{mod}/M corresponding to these modes decreases with an increase of f_c. On the contrary, the ratio M_{mod}/M for the oblique modes increases fastly with the growth of f_c and reaches the value of about 84% for f_c equal to 1000 Hz. These facts explain why the decay times are getting smaller with increasing of the cutoff frequency f_c.

The simulation results in Figs. 8 and 9 were gained when all modes with the natural frequencies from the frequency band $(0, f_c)$ were included in the RIR. However, the knowledge about the character of the sound decay, in particular, frequency bands such as octaves or one-third octaves is equally important. In this case a bandpass filtering of the RIR is realized by summing up such components of the series in Eq. (17) for which $f_l < f_{n_x n_y n_z} < f_u$, where f_l and f_u are the lower and upper limits of the frequency band. Using this procedure, temporal changes in the decay function L_d at the considered receiving points were computed for the octave bands with the centre frequency from 31.5 Hz to 1000 Hz, and the results are shown in Figs. 11 and 12. The simulation data obtained at the

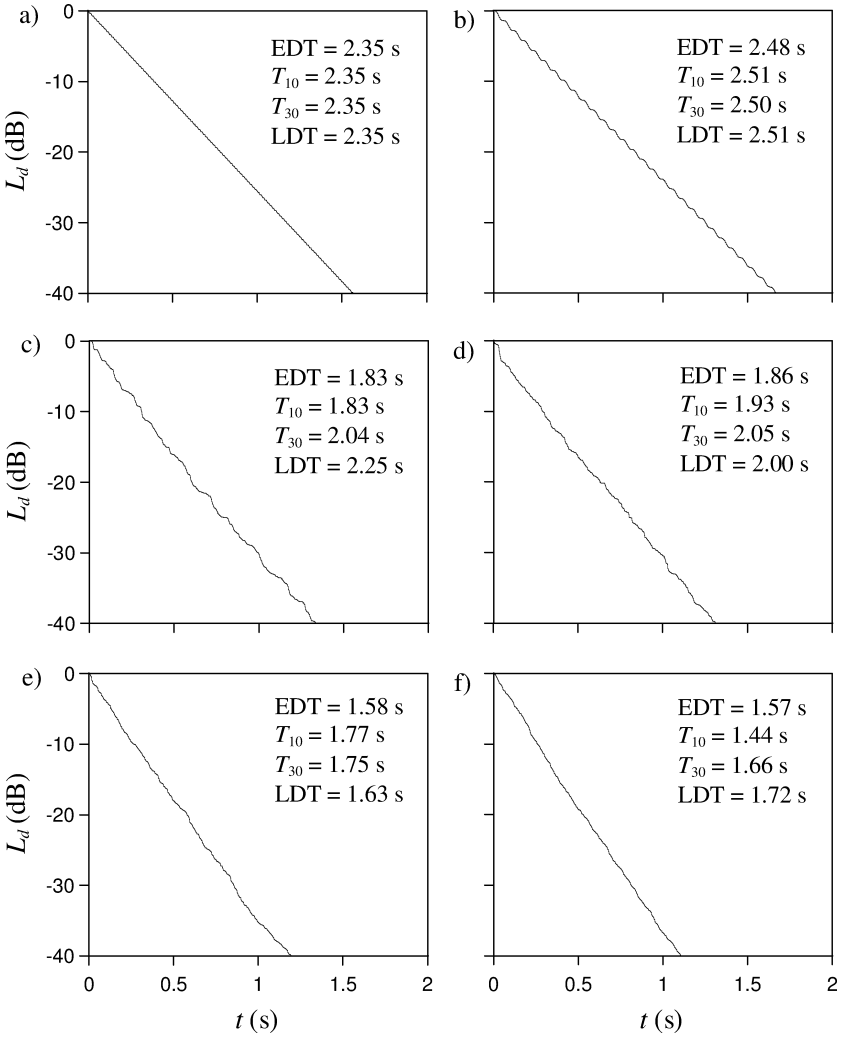

Fig. 11. Temporal changes in the decay function L_d at the receiving point: $x = 4$ m, $y = 2$ m, $z = 1.5$ m, for octave bands with the center frequency: a) 31.5 Hz, b) 63 Hz, c) 125 Hz, d) 250 Hz, e) 500 Hz, f) 1000 Hz.

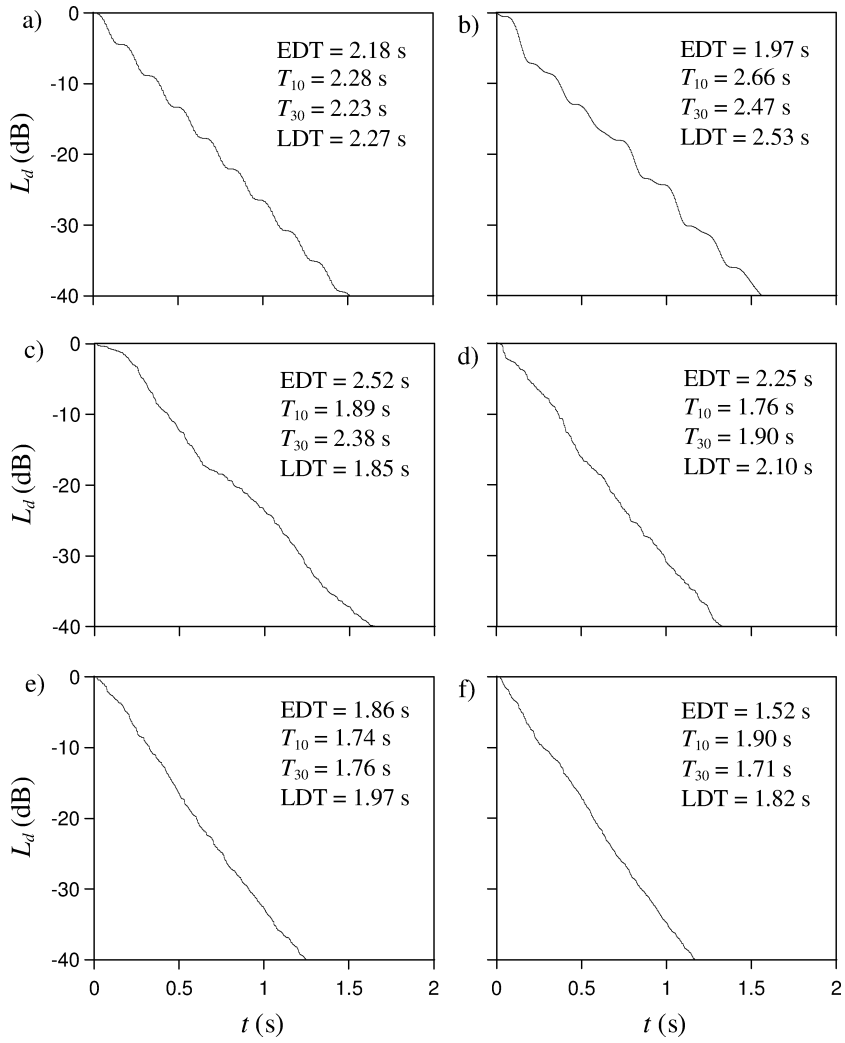

Fig. 12. Temporal changes in the decay function L_d at the receiving point: $x = 7$ m, $y = 4$ m, $z = 1.5$ m, for octave bands with the centre frequency: a) 31.5 Hz, b) 63 Hz, c) 125 Hz, d) 250 Hz, e) 500 Hz, f) 1000 Hz.

first receiving point can be easily interpreted because an inspection of the plots in Fig. 11 enables recognizing the sound decay as approximately exponential in each octave band. At the second receiving point a situation is different because the results in Fig. 12 discover a high influence of the frequency band on the character of the sound decay. For example, for the octave band with the centre frequency of 31.5 Hz wavy changes in L_d plot are observed (Fig. 12a) and this is due to a presence of sum and difference tones in the decay function (Eqs. (18)–(20)). On the other hand, for the octave bands with centre frequencies of 250 Hz, 500 Hz, and 1000 Hz the sound decay appears to be approximately exponential (Figs. 12d–f). However, for the remaining octave bands, changes in the decay function are highly nonlinear showing that in a rectangular room multiple-slope sound decays may also occur.

4. Summary and conclusions

Sound decay inside enclosures has been studied for many years because the decay times are the main parameters used for assessment of the acoustic quality of rooms. A method commonly used for predicting the indoor reverberation characteristics bases on the Schroeder backward integration of the squared RIR. The paper presents a novel method for a theoretical description of the sound decay in rooms including modelling of the RIR via the wave method and finding the decay function by the use of the Schroeder integration method. The method is designed for lightly damping rooms of an arbitrary shape. The modelling of the RIR was based on a solution of the wave equation in a series form whose components describe modal responses to the impulse source and a band-limitedness of the RIR results from a finiteness of this series. Theoretical

considerations have been accompanied with numerical simulations carried out for a rectangular room. The calculations have shown that the RIR can be used to reconstruct the structure of a sound field in an early stage of the sound decay and this reconstruction is more faithful when band-limitedness of the RIR becomes smaller. In order to properly characterize the reverberant properties of the room, four decay times: EDT, T_{10}, T_{30}, and LDT were calculated based on changes in the decay function. The simulation results have shown that distributions of decay times inside a room are highly irregular despite the fact that a uniform distribution of sound absorption by the room walls was assumed. Furthermore, these times decrease when band-limitedness of the RIR becomes smaller and this regularity results from increasing of the number of oblique modes in the RIR function. The simulation data obtained for the octave bands have demonstrated a high influence of the frequency band on the character of the sound decay and the predicted decay times. They also show that for some cases changes in the decay function are strongly nonlinear proving that even in a simple rectangular room multiple decay processes may occur.

References

1. Aretz M., Dietrich P., Vorländer M. (2014), *Application of the mirror source method for low frequency sound prediction in rectangular rooms*, Acta Acustica united with Acustica, **100**, 2, 306–319.
2. Bradley D., Wang L. (2005), *The effects of simple coupled volume geometry on the objective and subjective results from nonexponential decay*, Journal of the Acoustical Society of America, **118**, 3, 1480–1490.
3. Bradley D., Wang L. (2010), *Optimum absorption and aperture parameters for realistic coupled volume spaces determined from computational analysis and subjective testing results*, Journal of the Acoustical Society of America, **127**, 1, 223–232.
4. Collins P. (2006), *Differential and integral equations*, Oxford University Press, New York, Chap. 4.1.
5. Dance S., Roberts J., Shield B. (1995), *Computer prediction of sound distribution in enclosed spaces using an interference pressure model*, Journal of Sound and Vibration, **44**, 1, 53–65.
6. Dance S., Van Buuren G. (2013), *Effects of damping on the low-frequency acoustics of listening rooms based on an analytical model*, Journal of Sound and Vibration, **332**, 25, 6891–6904.
7. Dowell E., Gorman III G., Smith D. (1977), *Acoustoelasticity: general theory, acoustic natural modes and forced response to sinusoidal excitation, including comparison to experiment*, Journal of Sound and Vibration, **52**, 2, 519–542.
8. Dowell E. (1978), *Reverberation time, absorption, and impedance*, Journal of the Acoustical Society of America, **64**, 1, 181–191.
9. Easwaran V., Craggs A. (1996a), *An application of acoustic finite element models to finding the reverberation times of irregular rooms*, Acustica, **82**, 1, 54–64.
10. Easwaran V., Craggs A. (1996b), *Transient response of lightly damped rooms: A finite element approach*, Journal of the Acoustical Society of America, **99**, 1, 108–113.
11. Ermann M. (2007) *Double sloped decay: subjective listening test to determine perceptibility and preference*, Building Acoustics, **14**, 2, 91–108.
12. Félix S., Asch M., Filoche M., Sapoval B. (2007), *Localization and increased damping in irregular acoustic cavities*, Journal of Sound and Vibration, **299**, 4-5, 965–976.
13. Franzoni L., Bliss D., Rouse J. (2001), *An acoustic boundary element method based on energy and intensity variables for prediction of high-frequency broadband sound fields*, Journal of the Acoustical Society of America, **110**, 6, 3071–3080.
14. Funkhouser T., Tsingos N., Carlbom I., Elko G., Sondhi M., West J., Pingali G., Min P., Ngan A. (2004), *A beam tracing method for interactive architectural acoustics*, Journal of the Acoustical Society of America, **115**, 1, 739–756.
15. ISO 3382 (2012), *Acoustics – Measurement of room acoustic parameters. Part 1: Performance spaces. Part 2: Reverberation time in ordinary rooms*, International Organization for Standardization, Géneve.
16. Kinsler L., Frey A., Coppens A., Sander J. (2000), *Fundamentals of acoustics*, 4th. ed., John Wiley & Sons, New York, p. 351.
17. Kubota Y., Dowell E. (1992) *Asymptotic modal analysis for sound fields of a reverberant chamber*, Journal of the Acoustical Society of America, **92**, 2, 1106–1112.
18. Kuttruff H. (2009), *Room acoustics*, 5th ed., Spon Press, New York, pp. 78, 95, 98.
19. Laine S., Siltanen S., Lokki T., Savioja L. (2009), *Accelerated beam tracing algorithm*, Applied Acoustics, **70**, 1, 172–181.
20. Lehmann E., Johansson A. (2009), *Prediction of energy decay in room impulse responses simulated with an image-source model*, Journal of the Acoustical Society of America, **124**, 1, 269–277.
21. Li Y., Cheng L. (2004), *Modifications of acoustic modes and coupling due to a leaning wall in a rectangular cavity*, Journal of the Acoustical Society of America, **116**, 6, 3312–3318.
22. López J., Carnicero D., Ferrando N., Escolano J. (2013), *Parallelization of the finite-difference time-domain method for room acoustics modelling based on CUDA*, Mathematical and Computer Modelling, **57**, 7–8, 1822–1831.

23. Luizard P., Polack J-P., Katz B. (2014), *Sound energy decay in coupled spaces using a parametric analytical solution of a diffusion equation*, Journal of the Acoustical Society of America, **135**, 5, 2765–2776.

24. Mechel F. (2002), *Improved mirror source method in room acoustics*, Journal of Sound and Vibration, **256**, 5, 873–940.

25. Meissner M. (2009a), *Computer modelling of coupled spaces: variations of eigenmodes frequency due to a change in coupling area*, Archives of Acoustics, **34**, 2, 157–168.

26. Meissner M. (2009b), *Spectral characteristics and localization of modes in acoustically coupled enclosures*, Acta Acustica united with Acustica, **95**, 2, 300–305.

27. Meissner M. (2010), *Simulation of acoustical properties of coupled rooms using numerical technique based on modal expansion*, Acta Physica Polonica A, **118**, 1, 123–127.

28. Meissner M. (2012), *Acoustic energy density distribution and sound intensity vector field inside coupled spaces*, Journal of the Acoustical Society of America, **132**, 1, 228–238.

29. Meissner M. (2013a), *Evaluation of decay times from noisy room responses with pure-tone excitation*, Archives of Acoustics, **38**, 1, 47–54.

30. Meissner M. (2013b), *Acoustic behaviour of lightly damped rooms*, Acta Acustica united with Acustica, **99**, 5, 845–847.

31. Meissner M. (2015a), *Numerical investigation of sound field in enclosures: Evaluation of active and reactive components of sound intensity*, Journal of Sound and Vibration, **338**, 154–168.

32. Meissner M. (2015b), *Theoretical and numerical determination of low-frequency reverberant characteristics of coupled rooms*, Journal of Vibration and Acoustics-Transactions of the ASME, **137**, 4, 041013-1–9.

33. Morse P., Bolt R. (1944), *Sound waves in rooms*, Reviews of Modern Physics, **16**, 2, 69–150.

34. Morse P., Feshbach H. (1953), *Methods of theoretical physics*, McGraw-Hill, New York, pp. 804, 837.

35. Murphy D., Southern A., Savioja L. (2014), *Source excitation strategies for obtaining impulse responses in finite difference time domain room acoustics simulation*, Applied Acoustics, **82**, 6–14.

36. Okuzono T., Otsuru T., Tomiku R., Okamoto N. (2014), *A finite-element method using dispersion reduced spline elements for room acoustics simulation*, Applied Acoustics, **79**, 1–8.

37. Raghuvanshi N., Narain R., Lin M. (2009), *Efficient and accurate sound propagation using adaptive rectangular decomposition*, IEEE Transactions on Visualization and Computer Graphics, **15**, 5, 789–801.

38. Sakamoto S., Nagatomo H., Ushiyama A., Tachibana H. (2008), *Calculation of impulse responses and acoustic parameters in a hall by the finite-difference time-domain method*, Acoustical Science and Technology, **29**, 4, 256–265.

39. Sakuma T., Yasuda Y. (2002), *Fast multipole boundary element method for large-scale steady-state sound field analysis. Part I: setup and validation*, Acta Acustica united with Acustica, **88**, 4, 513–525.

40. Schroeder M. (1965), *New method of measuring reverberation time*, Journal of the Acoustical Society of America, **37**, 3, 400–412.

41. Schroeder M. (1996), *The "Schroeder frequency" revisited*, Journal of the Acoustical Society of America, **99**, 5, 3240–3241.

42. Skålevik M. (2011), *Schroeder frequency revisited*, Proceedings of Forum Acusticum 2011, Aalborg, Denmark.

43. Spa C., Garriga A., Escolano J. (2010), *Impedance boundary conditions for pseudo-spectral time-domain methods in room acoustics*, Applied Acoustics, **71**, 6, 402–410.

44. Sum K., Pan J. (2006), *Geometrical perturbation of an inclined wall on decay times of acoustic modes in a trapezoidal cavity with an impedance surface*, Journal of the Acoustical Society of America, **120**, 6, 3730–3743.

45. Summers J., Torres R., Shimizu Y. (2004), *Statistical-acoustics models of energy decay in systems of coupled rooms and their relation to geometrical acoustics*, Journal of the Acoustical Society of America, **116**, 2, 958–969.

46. Summers J., Torres R., Shimizu Y., Dalenbäk B. (2005), *Adapting a randomized beam-axis-tracing algorithm to modeling of coupled rooms via late-part ray tracing*, Journal of the Acoustical Society of America, **118**, 3, 1491–1502.

47. Summers J. (2012), *Accounting for delay of energy transfer between coupled rooms in statistical-acoustics models of reverberant-energy decay*, Journal of the Acoustical Society of America, **132**, 2, 129–134.

48. Szemela K. (2015), *Sound radiation from a surface source located at the bottom of the wedge region*, Archives of Acoustics, **40**, 2, 223–234.

49. Xiang N., Yun Jing Y., Bockman A. (2009), *Investigation of acoustically coupled enclosures using a diffusion-equation model*, Journal of the Acoustical Society of America, **126**, 3, 1187–1198.

50. Xu B., Sommerfeldt S. (2010), *A hybrid modal analysis for enclosed sound fields*, Journal of the Acoustical Society of America, **128**, 5, 2857–2867.